

Nonlinear Dendritic Coincidence Detection for Supervised Learning

Fabian Schubert^{1,*} and Claudius Gros¹

¹*Institute for Theoretical Physics, Goethe University Frankfurt am Main, Germany*

Correspondence*:

Institute for Theoretical Physics
Goethe University Frankfurt am Main
Max-von-Laue-Str. 1
60438 Frankfurt am Main, Germany
fschubert@itp.uni-frankfurt.de

2 ABSTRACT

Cortical pyramidal neurons have a complex dendritic anatomy, whose function is an active research field. In particular, the segregation between its soma and the apical dendritic tree is believed to play an active role in processing feed-forward sensory information and top-down or feedback signals. In this work, we use a simple two-compartment model accounting for the nonlinear interactions between basal and apical input streams and show that standard unsupervised Hebbian learning rules in the basal compartment allow the neuron to align the feed-forward basal input with top-down target signal received by the apical compartment. We show that this learning process, termed coincidence detection, is robust against strong distractions in the basal input space and demonstrate its effectiveness in a linear classification task.

Keywords: Dendrites, Pyramidal Neuron, Plasticity, Coincidence Detection, Supervised Learning

1 INTRODUCTION

In recent years, a growing body of research has addressed the functional implications of the distinct physiology and anatomy of cortical pyramidal neurons (Spruston, 2008; Hay et al., 2011; Ramaswamy and Markram, 2015). In particular, on the theoretical side, we saw a paradigm shift from treating neurons as point-like electrical structures towards embracing the entire dendritic structure (Larkum et al., 2009; Poirazi, 2009; Shai et al., 2015a). This was mostly due to the fact that experimental work uncovered dynamical properties of pyramidal neuronal cells that simply could not be accounted for by point models (Spruston et al., 1995; Häusser et al., 2000).

An important finding is that the apical dendritic tree of cortical pyramidal neurons can act as a separate nonlinear synaptic integration zone (Spruston, 2008; Branco and Häusser, 2011). Under certain conditions, a dendritic Ca^{2+} spike can be elicited that propagates towards the soma, causing rapid, bursting spiking activity. One of the cases in which dendritic spiking can occur was termed ‘backpropagation-activated Ca^{2+} spike firing’ (‘BAC firing’): A single somatic spike can backpropagate towards the apical spike initiation zone, in turn significantly facilitating the initiation of a dendritic spike (Stuart and Häusser, 2001; Spruston, 2008; Larkum, 2013). This reciprocal coupling is believed to act as a form of coincidence detection: If apical and basal synaptic input co-occurs, the neuron can respond with a rapid burst of spiking activity. The firing rate of these temporal bursts exceeds the firing rate that is maximally achievable under basal

synaptic input alone, therefore representing a form of temporal coincidence detection between apical and basal input.

Naturally, these mechanisms also affect plasticity and thus learning within the cortex (Sjöström and Häusser, 2006; Ebner et al., 2019). While the interplay between basal and apical stimulation and its effect on synaptic efficacies is subject to ongoing research, there is evidence that BAC-firing tends to shift plasticity towards long-term potentiation (LTP) (Letzkus et al., 2006). Thus, coincidence between basal and apical input appears to also gate synaptic plasticity.

In a supervised learning scheme, where the top down input arriving at the apical compartment acts as the teaching signal, the most straight-forward learning rule for the basal synaptic weights would be derived from an appropriate loss function, such as a mean square error, based on the difference between basal and apical input, i.e. $I_p - I_d$, where indices p and d denote ‘proximal’ and ‘distal’, in equivalence to basal and apical. Theoretical studies have investigated possible learning mechanisms that could utilize an intracellular error signal (Urbanczik and Senn, 2014; Schiess et al., 2016; Guerguiev et al., 2017). However, a clear experimental evidence for a physical quantity encoding such an error is—to our knowledge—yet to be found. On the other hand, Hebbian-type plasticity is extensively documented in experiments (Gustafsson et al., 1987; Debanne et al., 1994; Markram et al., 1997; Bi and Poo, 1998). Therefore, our work is based on the question whether the non-linear interactions between basal and apical synaptic input could, when combined with a Hebbian plasticity rule, allow a neuron to learn to reproduce an apical teaching signal in its proximal input.

We investigate coincidence learning by combining a phenomenological model that generates the output firing rate as a function of two streams of synaptic input (subsuming basal and apical inputs) with classical Hebbian, as well as BCM-like plasticity rules on basal synapses. In particular we hypothesized that this combination of neural activation and plasticity rules would lead to an increased correlation between basal and apical inputs. Furthermore, the temporal alignment observed in our study could potentially facilitate apical inputs to act as top-down teaching signals, without the need for an explicit error-driven learning rule. Thus, we also test our model in a simple linear supervised classification task and compare it with the performance of a simple point neuron equipped with similar plasticity rules.

2 MODEL

2.1 Compartamental Neuron

The neuron model used throughout this study is a discrete-time rate encoding model that contains two separate input variables, subsuming the total synaptic input current injected arriving at the basal (proximal) and apical (distal) dendritic structure of a pyramidal neuron, respectively. The model is a slightly simplified version of a phenomenological model proposed by Shai et al. (2015b). Denoting the input currents I_p (proximal) and I_d (distal), the model is written as

$$y(t) = \alpha \sigma(I_p(t) - \theta_{p0}) [1 - \sigma(I_d(t) - \theta_d)] + \sigma(I_d(t) - \theta_d) \sigma(I_p(t) - \theta_{p1}) \quad (1)$$

$$\sigma(x) \equiv \frac{1}{1 + \exp(-4x)} . \quad (2)$$

Here, $\theta_{p0} > \theta_{p1}$ and θ_d are threshold variables with respect to proximal and distal inputs. Overall, equation (1) describes two distinct regions of neural activation in the (I_p, I_d) -space which differ in their maximal firing rates, which are set to 1 and α , where $0 < \alpha < 1$. A plot of (1) is shown in Fig. 1.

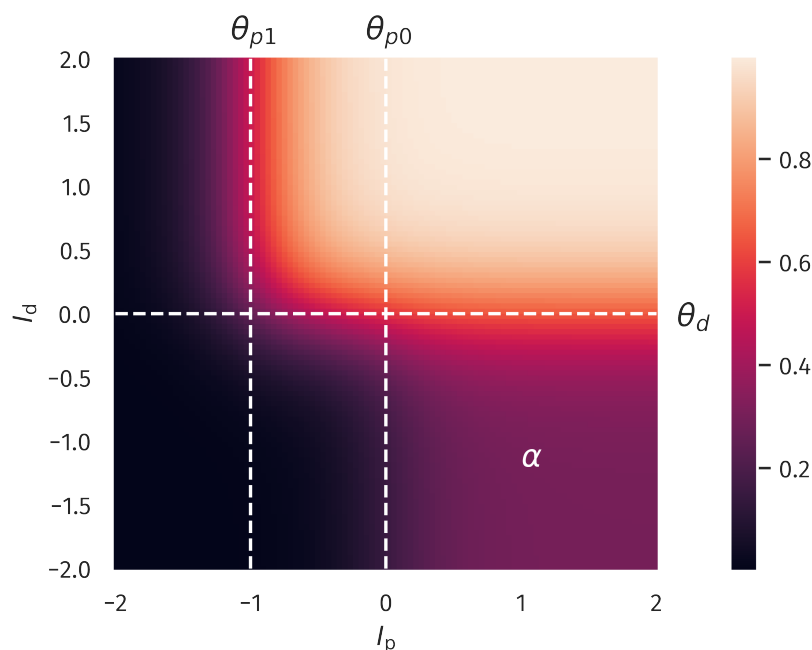


Figure 1. Two-compartment rate model. The firing rate as a function of proximal and distal inputs I_p and I_d , see (1). The thresholds θ_{p0} , θ_{p1} and θ_d define two regions of neural activity, with a maximal firing rate of unity and a plateau at $\alpha = 0.3$.

When both input currents I_d and I_p are large, viz larger than the thresholds θ_d and θ_{p1} , the second term in (1) dominates, which leads to $y \approx 1$. An intermediate activity plateau, of strength α emerges in addition when $I_p > \theta_{p0}$ and $I_d < \theta_d$. As such, the compartment model (1) is able to distinguish neurons with a normal activity level, here encoded by $\alpha = 0.3$, and strongly bursting neurons, where the maximal firing rate is unity. The intermediate plateau allows neurons to process the proximal inputs I_p even in the absence of distal stimulation. The distal current I_d acts therefore as an additional modulator.

In our numerical experiments we compare the compartment model with a classical point neuron, as given by

$$y(t) = \sigma(I_p(t) + I_d(t) - \theta) . \quad (3)$$

The apical input I_d is generated ‘as is’, meaning, it is not dynamically calculated as a superposition of multiple presynaptic inputs. For concreteness, we used

$$I_d(t) = n_d(t)x_d(t) - b_d(t) , \quad (4)$$

where $n_d(t)$ is a scaling factor, $x_d(t)$ a pre-generated discrete time sequence and $b_d(t)$ a bias. Note that n_d and b_d are time dependent since they are subject to adaptation processes, which will be described in the next section. Similarly, the proximal input $I_p(t)$ is given by

$$I_p(t) = n_p(t) \sum_{i=1}^N x_{p,i}(t)w_i(t) - b_p(t) , \quad (5)$$

where N is the number of presynaptic afferents, $x_{p,i}(t)$ the corresponding sequences, $w_i(t)$ the synaptic efficacies and $n_p(t)$ and $b_p(t)$ the (time dependent) scaling and bias. Typical values for the parameters used throughout this study are presented in Table 1.

76 2.2 Homeostatic Parameter Regulation

The bias variables entering the definitions (4) and (5) of the distal proximal current, I_d and I_p , are assumed to adapt according to

$$b_p(t+1) = b_p(t) + \mu_b [I_p(t) - I_p^t] \quad (6)$$

$$b_d(t+1) = b_d(t) + \mu_b [I_d(t) - I_d^t] , \quad (7)$$

77 where $I_p^t = 0$ and, $I_d^t = 0$ are preset targets and $1/\mu_b = 10^3$ the timescale for the adaption process. Over
78 time, both the distal and the proximal currents, I_d and I_p , average out.

Adaptation rules for the bias entering a transfer function, such as (7) and (6), have the task to regulate overall activity levels. The overall magnitude of the synaptic weights, which are determined by synaptic rescaling factors, here n_d and n_p , as defined in (4) and (5), will regulate in contrast the variance of the neural activity, and not the average level (Schubert and Gros, 2021). In this spirit we consider

$$n_d(t+1) = n_d(t) + \mu_n \left[V_d^t - \left(I_d(t) - \tilde{I}_d(t) \right)^2 \right] \quad (8)$$

$$n_p(t+1) = n_p(t) + \mu_n \left[V_p^t - \left(I_p(t) - \tilde{I}_p(t) \right)^2 \right] \quad (9)$$

$$\tilde{I}_d(t+1) = (1 - \mu_{av})\tilde{I}_d(t) + \mu_{av}I_d(t) \quad (10)$$

$$\tilde{I}_p(t+1) = (1 - \mu_{av})\tilde{I}_p(t) + \mu_{av}I_p(t) \quad (11)$$

79 Here, V_p^t and V_d^t define targets for the temporal averaged variances of I_p and I_d . The dynamic variables \tilde{I}_p
80 and \tilde{I}_d are simply low-pass filtered running averages of I_p and I_d . Overall, the framework specified here
81 allows the neuron to be fully flexible, as long as the activity level and its variance fluctuate around preset
82 target values (Schubert and Gros, 2021). A list of the parameter values used throughout this investigation is
83 also given in Table 1. Our choices of target means and variances are based on the assumption that neural
84 input should be tuned towards a certain working regime of the neural transfer function. In the case of the
85 presented model, this means that both proximal and distal input cover an area where the nonlinearities of
86 the transfer function are reflected without oversaturation.

Table 1. Model parameters, as defined in sections 2.1 and 2.3.

θ_{p0}	0	V_d^t	0.25
θ_{p1}	-1	μ_b	10^{-3}
θ_d	0	μ_n	10^{-4}
α	0.3	μ_{av}	$5 \cdot 10^{-3}$
μ_w	$5 \cdot 10^{-5}$	I_p^t	0
ϵ	0.1	I_d^t	0
V_p^t	0.25		

87 2.3 Synaptic Plasticity

The standard Hebbian plasticity rule for the proximal synaptic weights is given by

$$w_i(t+1) = w_i(t) + \mu_w [(x_{p,i}(t) - \tilde{x}_{p,i}(t)) (y(t) - \tilde{y}) - \epsilon w_i(t)] \quad (12)$$

$$\tilde{x}_{p,i}(t+1) = (1 - \mu_{av})\tilde{x}_{p,i}(t) + \mu_{av}x_{p,i}(t) \quad (13)$$

$$\tilde{y}(t+1) = (1 - \mu_{av})\tilde{y}(t) + \mu_{av}y(t) \quad (14)$$

88 The trailing time averages $\tilde{x}_{p,i}$ and \tilde{y} , respectively of the presynaptic basal activities, $x_{p,i}$, and of the neural
89 firing rate y , enter the Hebbian learning rule (12) as reference levels. Pre- and post-synaptic neurons are
90 considered to be active/inactive when being above/below the respective trailing averages. The timescale
91 of the averaging, $1/\mu_{av}$, is typically over 200 time steps, see Table 1. Since classical Hebbian learning
92 does not keep weights bounded, we use an additional proportional decay term ϵw_i which prevents runaway
93 growth using $\epsilon = 0.1$. With $1/\mu_w = 2 \cdot 10^4$, learning is assumed to be considerably slower, as usual for
94 statistical update rules. For comparative reasons, the point neuron model (3) is equipped with the same
95 plasticity rule for the proximal weights as (12).

96 Apart from classical Hebbian learning, we also considered a BCM-like learning rule for the basal weights
97 (Bienenstock et al., 1982; Intrator and Cooper, 1992). The form of the BCM-rule used here reads

$$w_i(t+1) = w_i(t) + \mu_w [y(y - \theta_M)x_i - \epsilon w_i] , \quad (15)$$

98 where θ_M is a threshold defining a transition from long-term potentiation (LTP) to long-term depression
99 (LTD) and, again, ϵ is a decay term on the weights preventing unbounded growth. In the variant introduced
100 by Law and Cooper (1994), the sliding threshold is simply the temporal average of the squared neural
101 activity, $\theta_M = \langle y^2 \rangle$. In practice, this would be calculated as a running average, thereby preventing the
102 weights from growing indefinitely.

103 However, for our compartment model, we chose to explicitly set the threshold to be the mean value
104 between the high- and low-activity regime in our compartment model, i.e. $\theta_M = (1 + \alpha)/2$. By doing
105 so, LTP is preferably induced if both basal and apical input are present at the same time. Obviously, for
106 the point model, the reasoning behind our choice of θ_M did not apply. Still, to provide some level of
107 comparability, we also ran simulations with a point model where the sliding threshold was calculated as a
108 running average of y^2 .

3 RESULTS

109 3.1 Unsupervised Alignment between Basal and Apical Inputs

110 As a first test, we quantify the neuron's ability to align its basal input to the apical teaching signal. This
111 can be done using the pearson correlation coefficient $\rho[I_p, I_d]$ between the basal and apical input currents.
112 We determined $\rho[I_p, I_d]$ after the simulation, which involves all plasticity mechanisms, both for the synaptic
113 weights and for the intrinsic parameters. The input sequences $x_{p,i}(t)$ is randomly drawn from a uniform
114 distribution, in $[0, 1]$, which is done independently for each $i \in [1, N]$.

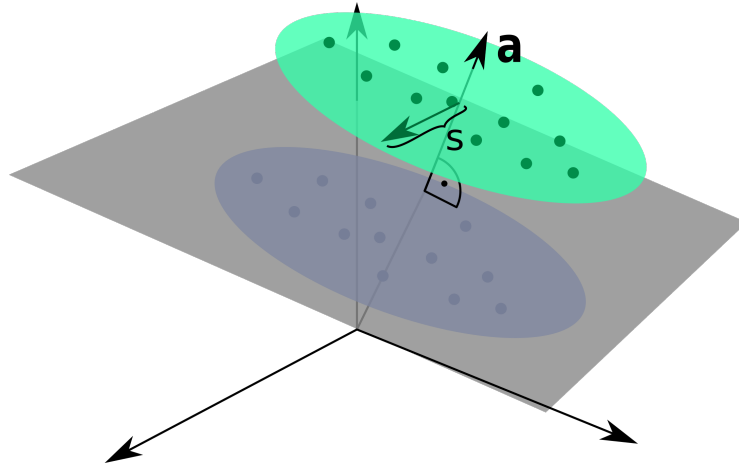


Figure 2. Input Space for the Linear Classification Task. Two clusters of presynaptic basal activities were generated from multivariate Gaussian distributions. Here, s denotes the standard deviation orthogonal to the normal vector \mathbf{a} of the classification hyperplane, as defined by (16).

For the distal current $I_d(t)$ to be fully ‘reconstructable’ by the basal input, $x_d(t)$ has to be a linear combination

$$x_d(t) = \sum_{i=1}^N a_i x_{p,i}(t) \quad (16)$$

of the $x_{p,i}(t)$, where the a_i are the components of a random vector \mathbf{a} of unit length.

Given that we use with (12) a Hebbian learning scheme, one can expect that the direction and the magnitude of the principal components of the basal input may affect the outcome of the simulation significantly: A large variance in the basal input orthogonal to the ‘reconstruction vector’ \mathbf{a} is a distraction for the plasticity. The observed temporal alignment between I_p and I_d should hence suffer when such a distraction is present.

In order to test the effects of distracting directions, we applied a transformation to the input sequences $x_{p,i}(t)$. For the transformation, two parameters are used, a scaling factor s and the dimension N_{dist} of the distracting subspace within the basal input space. The N_{dist} randomly generated basis vectors are orthogonal to the superposition vector \mathbf{a} , as defined by (16), and to each others. Within this N_{dist} -dimensional subspace, the input sequences $x_{p,i}(t)$ are rescaled subsequently by the factor s . After the learning phase, a second set of input sequences $x_{p,i}(t)$ and $x_d(t)$ is generated for testing purposes, using the identical protocol, and the cross correlation $\rho[I_p, I_d]$ evaluated. During the testing phase plasticity is turned off.

The overall aim of our portocal is to evaluate the degree $\rho[I_p, I_d]$ to which the proximal current I_p aligns in the temporal domain to the distal input I_d . We recall that this is a highly non-trivial question, given that the proximal synpatic weights are adapted via Hebbian plasticity, see (12). The error $(I_p - I_d)^2$ does not enter the adaption rules employed. Results are presented in Fig. 3 as a function of the distraction parameters s and $N_{\text{dist}} \in [0, N - 1]$. The total number of basal inputs is $N = 100$.

For a comparison, in Fig. 3 data for both the compartment model and for a point neuron are presented (as defined respectively by (1) and (3)), as well as results for both classical Hebbian and BCM learning rules. A decorrelation transition as a function of the distraction scaling paramerer s is observed for both models and plasticity rules. In terms of the learning rules, only marginal differences are present. However, the

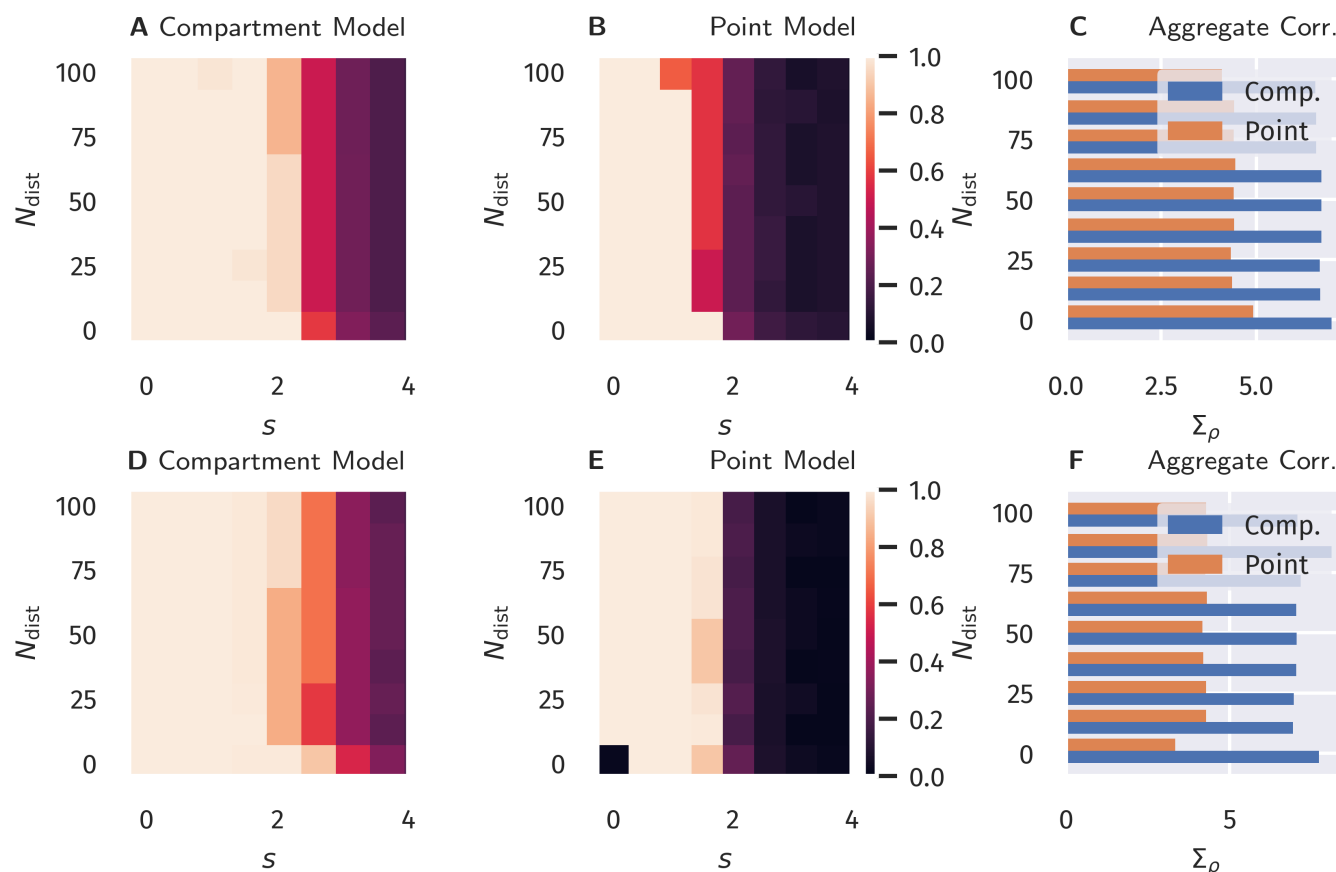


Figure 3. Unsupervised Alignment between Basal and Apical Input. Color encoded is the Pearson correlation $\rho[I_p, I_d]$ between the proximal and distal input currents, I_p and I_d . A–C: Classical Hebbian plasticity, as defined by (12). D–F: BCM rule, see (15). Data for a range $N_{\text{dist}} \in [0, N - 1]$ of the orthogonal distraction directions, and scaling factors s , as defined in Fig. 2. The overall number of basal inputs is $N = 100$. In the bar plot on the right the sum Σ_{acc} over $s = 0, 0.5, 1.0 \dots$ of the results is shown as a function of N_{dist} . Blue bars represents the compartment model, orange the point model.

compartment model is able to handle a significantly stronger distraction as compared to the point model. These findings support the hypothesis examined here, namely that nonlinear interactions between basal and apical input improve learning guided by top-down signals.

3.2 Supervised Learning in a Linear Classification Task

Next, we investigated if the observed differences would also improve the performance in an actual supervised learning task. For this purpose, we constructed presynaptic basal input $x_p(t)$ as illustrated in Fig. 2. Written in vector form, each sample from the basal input is generated from,

$$\mathbf{x}_p(t) = \mathbf{b} + \mathbf{a}[c(t) + \sigma_a \zeta_a(t)] + s \cdot \sum_{i=1}^{N_{\text{dist}}} \zeta_{\text{dist},i}(t) \mathbf{v}_{\text{dist},i}, \quad (17)$$

where \mathbf{b} is a random vector drawn uniformly from $(0, 1)^N$, \mathbf{a} is random unit vector as introduced in Section 3.1, $c(t)$ is a binary variable drawn from $\{-0.5, 0.5\}$ with equal probability and $\zeta_a(t)$ and the $\zeta_{\text{dist},i}(t)$ are independent random Gaussian variables with zero mean and unit variance. Hence, σ_a simply denotes the standard deviation of each Gaussian cluster along the direction of the normal vector \mathbf{a} and was set to $\sigma_a = 0.25$. Finally, the set of $\mathbf{v}_{\text{dist},i}$ forms a randomly generated orthogonal basis of N_{dist}

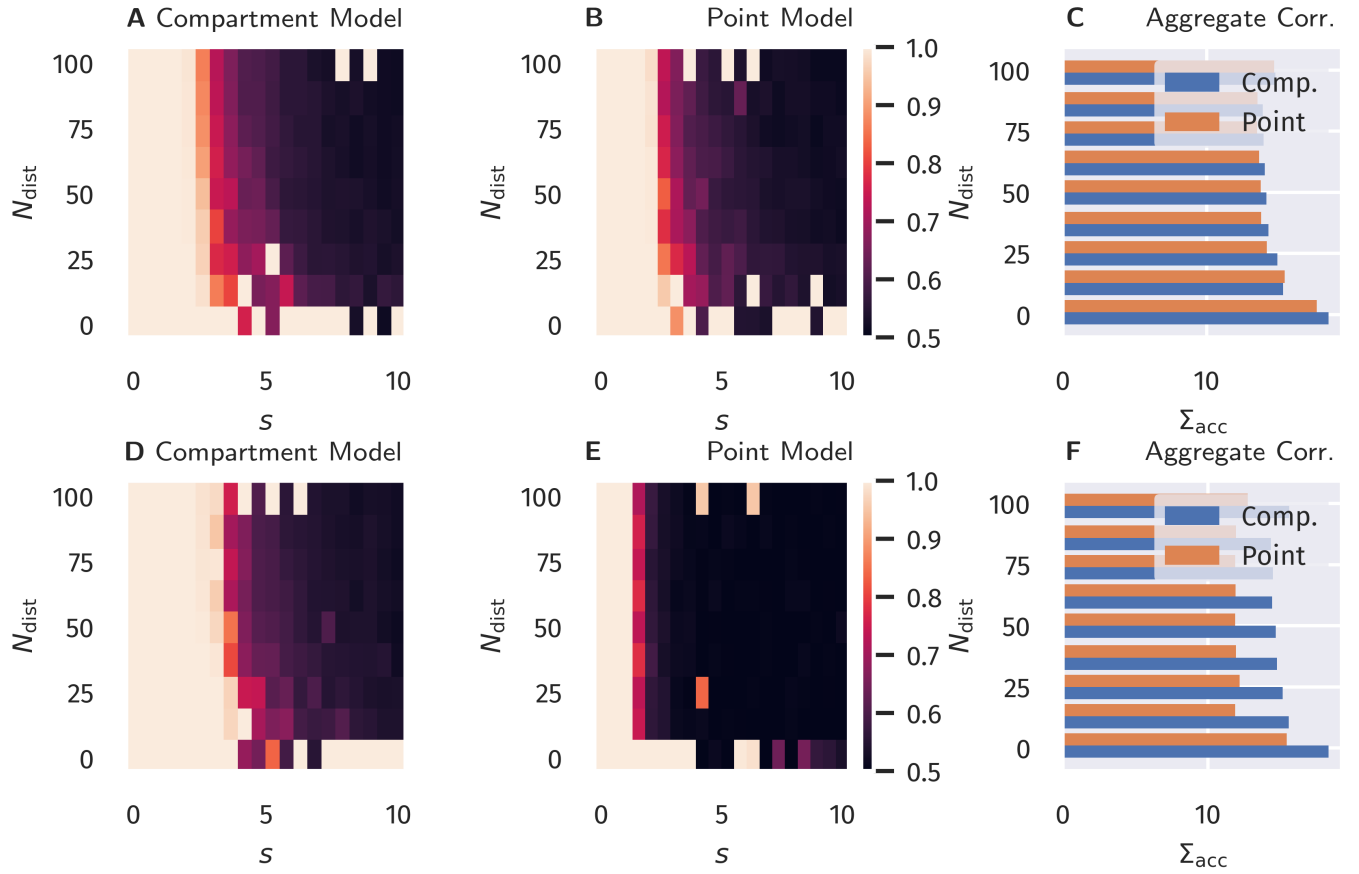


Figure 4. Binary Classification Accuracy. Fraction of correctly classified patterns as illustrated in Fig. 2, see Section 3.2. A–C: Classical Hebbian plasticity. D–F: BCM rule. In the bar plot on the right the sum Σ_{acc} over $s = 0, 0.5, 1.0$ of the results is given as a function of N_{dist} . Blue bars represents the compartment model, orange the point model.

unit vectors which are—as in Section 3.1—also orthogonal to \mathbf{a} . The free parameter s parameterizes the standard deviation along this subspace orthogonal to \mathbf{a} . As indicated by the time dependence, the Gaussian and binary random variables are drawn for each time step. The vectors \mathbf{b} , \mathbf{a} , and $\mathbf{v}_{\text{dist},i}$ are generated once before the beginning of a simulation run.

For the classification task, we use two output neurons, indexed 0 and 1, receiving the same basal presynaptic input, with the respective top-down inputs $x_{d,0}$ and $x_{d,1}$ encoding the desired linear classification in a one-hot scheme,

$$x_{d,0}(t) = 1 - \Theta \left((\mathbf{x}_p(t) - \mathbf{b})^T \mathbf{a} \right) \quad (18)$$

$$x_{d,1}(t) = \Theta \left((\mathbf{x}_p(t) - \mathbf{b})^T \mathbf{a} \right), \quad (19)$$

where $\Theta(x)$ is the Heaviside step function.

As in the previous experiment, we ran a full simulation until all dynamic variables reached a stationary state. After this, a test run without plasticity and with the apical input turned off was used to evaluate the classification performance. For each sample, the index of the neuron with the highest activity was used as the predicted class. Accuracy was then calculated as the fraction of correctly classified samples.

158 The resulting accuracy as a function of N_{dist} and s is shown in Fig. 4, again for all four combinations of
159 neuron models and learning rules.

160 For classical Hebbian plasticity, the differences between compartmental and point neuron are small.
161 Interestingly, the compartment model performs measurably better in the case of the BCM rule (15), in
162 particular when the overall accuracies for the tested parameter range are compared, see Fig. 4D. This
163 indicates that the compartmental neuron makes better use, during learning, of the three distinct activity
164 plateaus at 0, α and 1, when the BCM rule is at work. Compare Fig. 1. We point out in this respect that the
165 sliding threshold θ_M in (15) has been set to the half-way point between the two non-trivial activity levels,
166 α and 1.

167 It should be noted that the advantage of the compartment model is also reflected in the actual correlation
168 between proximal and distal input as a measure of successful learning (as done in the previous section), see
169 Fig. 5 in the appendix. Interestingly, the discrepancies are more pronounced when measuring the correlation
170 as compared to the accuracy. Moreover, it appears that above-chance accuracy is still present for parameter
171 values where alignment is almost zero. We attribute this effect to the fact that the classification procedure
172 predicts the class by choosing the node that has the higher activity, independent of the actual “confidence”
173 of this prediction, i.e. how strong activities differ relative to their actual activity levels. Therefore, marginal
174 differences can still yield the correct classification in this isolated setup, but it would be easily disrupted by
175 finite levels of noise or additional external input.

4 DISCUSSION

176 The workhorse of the brain, pyramidal neurons, possess distinct apical/basal (distant/proximal) dendritic
177 trees. It is hence likely that models with at least two compartments are necessary for describing the
178 functionality of pyramidal neurons. For a proposed two-compartment transfer function (Shai et al., 2015b),
179 we have introduced both unsupervised and supervised learning schemes, showing that the two-compartment
180 neuron is significantly more robust against distracting components in the proximal input space than a
181 corresponding (one-compartment) point neuron.

182 The apical and basal dendritic compartments of pyramidal neurons are located in different cortical layers
183 Park et al. (2019), receiving top-down and feed-forward signals, respectively. The combined action of these
184 two compartments is hence the prime candidate for the realization of backpropagation in multi-layered
185 networks (Bengio, 2014; Lee et al., 2015; Guerguiev et al., 2017).

186 In the past, backpropagation algorithms for pyramidal neurons concentrated on learning rules that are
187 explicitly dependent on an error term, typically the difference between top-down and bottom up signals.
188 In this work, we considered an alternative approach. We postulate that the correlation between proximal
189 and distal input constitutes a viable objective function, which is to be maximized in combination with
190 homeostatic adaptation rules that keeps proximal and distal inputs within desired working regimes. Learning
191 correlations between distinct synaptic or compartmental inputs is as standard task for Hebbian-type learning,
192 which implies that the here proposed framework is based not on supervised, but on biologically viable
193 unsupervised learning schemes.

194 The proximal input current I_p is a linear projection of the proximal input space. Maximizing the
195 correlation between I_p and I_d (the distal current), can therefore be regarded as a form of canonical
196 correlation analysis (CCA) (Härdle and Simar, 2007). The idea of using CCA as a possible mode of
197 synaptic learning has previously been investigated by Haga and Fukai (2018). Interestingly, according to
198 the authors, a BCM-learning term in the plasticity dynamics accounts for a principal component analysis

199 in the input space, while CCA requires an additional multiplicative term between local basal and apical
 200 activity. In contrast, our results indicate that such a multiplicative term is not required to drive basal
 201 synaptic plasticity towards a maximal alignment between basal and apical input, even in the presence
 202 of distracting principal components. Apart from the advantage that this avoids the necessity of giving a
 203 biophysical interpretation of such cross-terms, it is also in line with the view that synaptic plasticity should
 204 be formulated in terms of local membrane voltage traces (Clopath et al., 2010; Weissenberger et al., 2018).
 205 According to this principle, distal compartments should therefore only implicitly affect plasticity in basal
 206 synapses, e.g. by facilitating spike initiation.

207 Here we concentrated on one-dimensional distal inputs. For the case of higher-dimensional distal input
 208 patterns, as for structured multi-layered networks, it thus remains to be investigated how target signals are
 209 formed. However, as previous works have indicated, random top-down weights are generically sufficient
 210 for successful credit assignment and learning tasks (Lillicrap et al., 2016; Guerguiev et al., 2017). We
 211 therefore expect that our results can be transferred also to deep network structures, for which plasticity is
 212 classically guided by local errors between top-down and bottom-up signals.

5 APPENDIX

213 5.1 Alignment in the Classification Task

214 Instead of measuring the model performance in the classification task presented in Sect. 3.2 by the
 215 fraction of correctly classified patterns, as shown in Fig. 4, one can also use the correlation between I_p
 216 and I_d , as done in Sect. 3.1. This is shown in Fig. 5. One observes a more pronounced difference between
 217 the point model and the compartment model, where the latter results in an overall better alignment for the
 218 tested parameter space.

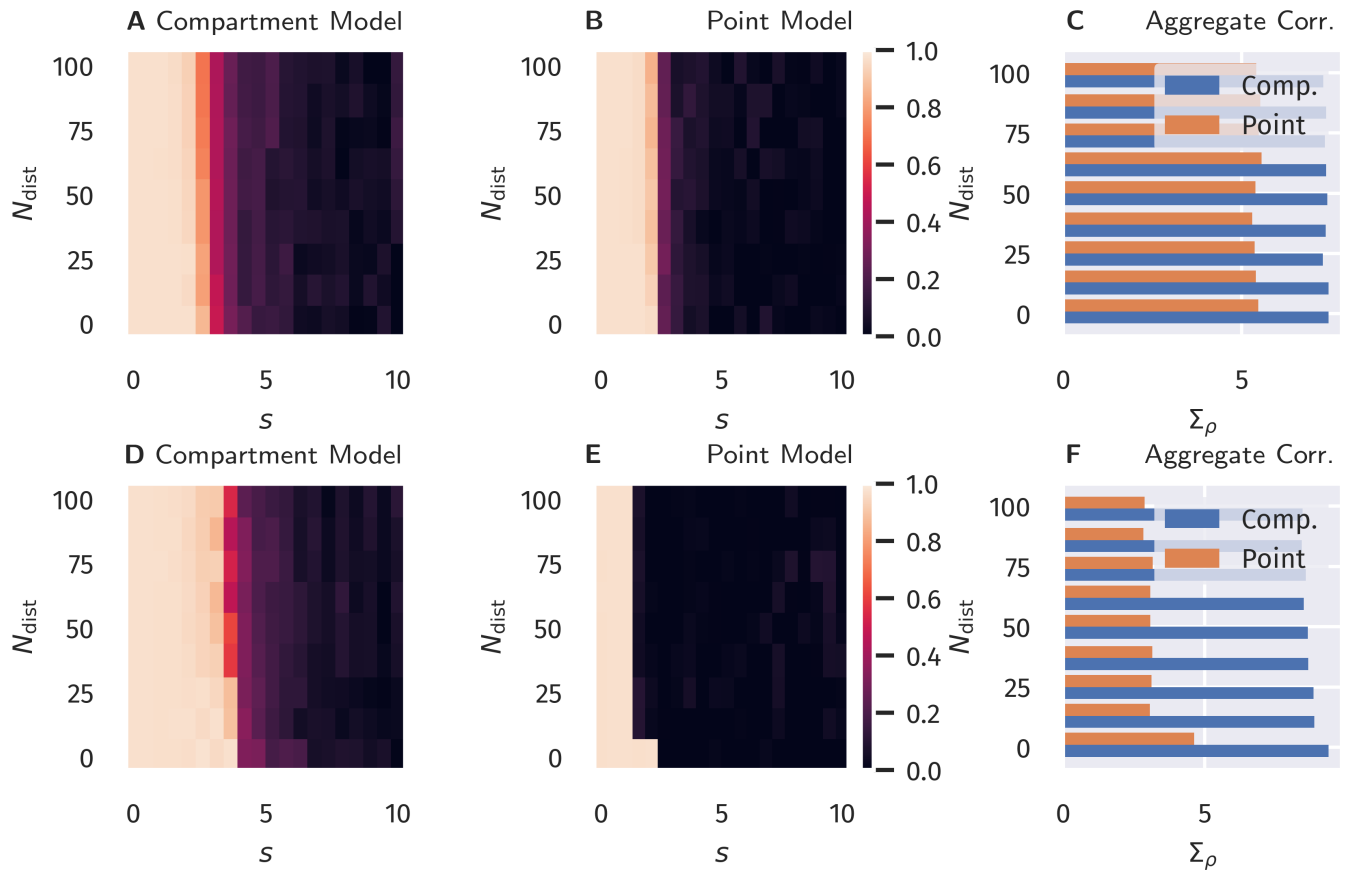


Figure 5. Alignment between Basal and Apical Input after Binary Classification Learning. Correlation between proximal and distal inputs after training, as described in Sect. 3.2. A–C: Classical Hebbian plasticity. D–F: BCM rule. In the bar plot on the right the sum Σ_{acc} over $s = 0, 0.5, 1.0$ of the results is shown as a function of N_{dist} . Blue bars represents the compartment model, orange the point model.

5.2 Objective Function of BCM Learning in the Compartment Model

To gain a better understanding of why the BCM-type learning rule in combination with the implemented compartment model drives the neuron towards the temporal alignment between I_p and I_d , we can formalize the learning rule for the proximal weights in terms of an objective function. For this purpose, we further simplify (1) by replacing the sigmoid functions $\sigma(x)$ by a simple step function $\Theta(x)$. This does not change the overall shape or topology of the activation in the (I_p, I_d) space but merely makes the smooth transitions sharp and instantaneous. Using $\Delta w_i \propto y(y - \theta_M)x_i$, we find in this case

$$\Delta w_i \propto \left[(1 - \alpha)\Theta(I_d - \theta_d)\Theta(p - \theta_{p1}) + \alpha(\alpha - 1)\Theta(\theta_d - I_d)\Theta(p - \theta_{p0}) \right] x_i. \quad (20)$$

Noting that $\Theta(x)$ is the first derivative of the ReLu function $[x]^+ \equiv \max(0, x)$, we find that this update rule can be written as

$$\begin{aligned} \Delta w_i &\propto \frac{\partial \mathcal{L}_p}{\partial w_i} \\ \mathcal{L}_p &= (1 - \alpha)\Theta(I_d - \theta_d)[p - \theta_{p1}]^+ + \alpha(\alpha - 1)\Theta(\theta_d - I_d)[p - \theta_{p0}]^+. \end{aligned} \quad (21)$$

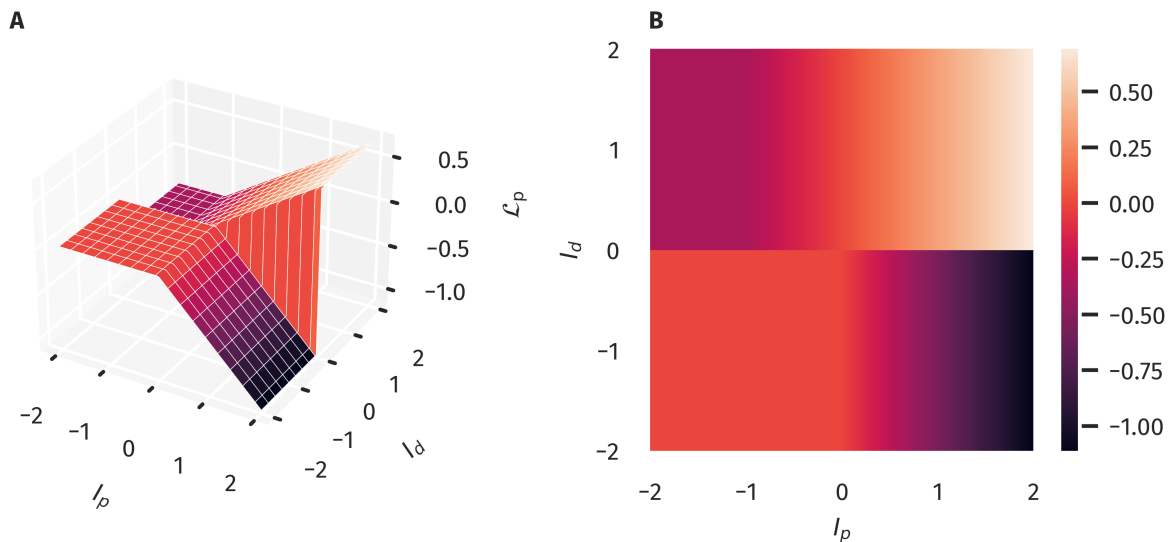


Figure 6. Objective Function for the Proximal Weight Update. The approximate objective function for the proximal weights as given in (21) as a 3d-plot (A) and color-coded (B). This corresponds to a combination of using (1) together with (15). Note the ridge-like structure along the I_p - I_d diagonal, which supports the alignment between proximal and distal input.

228 The objective function \mathcal{L}_p is shown in Fig. 6. One observes that states closer to the I_p - I_d diagonal are
 229 preferred since they tend to yield higher values of \mathcal{L}_p , while the opposite is the case for off-diagonal states.

230 It should be noted, though, that the objective function is not scale-invariant (as would be e.g. if the
 231 squared error was used) in the sense that the prior distributions of both proximal and distal inputs need
 232 a certain mean and variance to cover a region of input states for which the described effects can take
 233 place. As a counterexample, one could imagine that the input samples only covered a flat area of \mathcal{L}_p , as
 234 for example in Fig. 6B in the lower left quadrant, leading to a zero average gradient. This is prevented,
 235 however, by the homeostatic processes acting simultaneously on the gains and biases, making sure that
 236 the marginal distributions of I_p and I_d are such that higher correlations are preferred. For example, if we
 237 assume a Gaussian marginal distribution for both I_p and I_d with zero means and a standard deviation of 0.5
 238 (which is used as a homeostatic target in the simulations), the expected value of $\mathcal{L}(I_p, I_d)$ is -0.055 if I_p
 239 and I_d are completely uncorrelated, and 0.07 in the perfectly correlated case.

CONFLICT OF INTEREST STATEMENT

240 The authors declare that the research was conducted in the absence of any commercial or financial
 241 relationships that could be construed as a potential conflict of interest.

AUTHOR CONTRIBUTIONS

242 Both authors, F.S. and C.G., contributed equally to the writing and review of the manuscript. F.S. provided
 243 the code, ran the simulations and prepared the figures.

ACKNOWLEDGMENTS

244 The authors acknowledge the financial support of the German research foundation (DFG)

DATA AVAILABILITY STATEMENT

245 The datasets [GENERATED/ANALYZED] for this study can be found in the [NAME OF REPOSITORY]
246 [LINK].

REFERENCES

- 247 Bengio, Y. (2014). How Auto-Encoders Could Provide Credit Assignment in Deep Networks via Target
248 Propagation
- 249 Bi, G. Q. and Poo, M. M. (1998). Synaptic modifications in cultured hippocampal neurons: Dependence on
250 spike timing, synaptic strength, and postsynaptic cell type. *Journal of Neuroscience* 18, 10464–10472.
251 doi:10.1523/jneurosci.18-24-10464.1998
- 252 Bienenstock, E. L., Cooper, L. N., and Munro, P. W. (1982). Theory for the development of neuron
253 selectivity: Orientation specificity and binocular interaction in visual cortex. *Journal of Neuroscience* 2,
254 32–48. doi:10.1523/jneurosci.02-01-00032.1982
- 255 Branco, T. and Häusser, M. (2011). Synaptic Integration Gradients in Single Cortical Pyramidal Cell
256 Dendrites. *Neuron* 69, 885–892. doi:10.1016/j.neuron.2011.02.006
- 257 Clopath, C., Büsing, L., Vasilaki, E., and Gerstner, W. (2010). Connectivity reflects coding: A model of
258 voltage-based STDP with homeostasis. *Nature Neuroscience* 13, 344–352. doi:10.1038/nn.2479
- 259 Debanne, D., Gähwiler, B. H., and Thompson, S. M. (1994). Asynchronous pre- and postsynaptic activity
260 induces associative long-term depression in area CA1 of the rat hippocampus in vitro. *Proceedings of*
261 *the National Academy of Sciences of the United States of America* 91, 1148–1152. doi:10.1073/pnas.91.
262 3.1148
- 263 Ebner, C., Clopath, C., Jedlicka, P., and Cuntz, H. (2019). Unifying Long-Term Plasticity Rules for
264 Excitatory Synapses by Modeling Dendrites of Cortical Pyramidal Neurons. *Cell Reports* 29, 4295–
265 4307.e6. doi:10.1016/j.celrep.2019.11.068
- 266 Guerguiev, J., Lillicrap, T. P., and Richards, B. A. (2017). Towards deep learning with segregated dendrites.
267 *eLife* 6. doi:10.7554/eLife.22901
- 268 Gustafsson, B., Wigstrom, H., Abraham, W. C., and Huang, Y. Y. (1987). Long-term potentiation in the
269 hippocampus using depolarizing current pulses as the conditioning stimulus to single volley synaptic
270 potentials. *Journal of Neuroscience* 7, 774–780. doi:10.1523/jneurosci.07-03-00774.1987
- 271 Haga, T. and Fukai, T. (2018). Dendritic processing of spontaneous neuronal sequences for single-trial
272 learning. *Scientific Reports* 8, 15166. doi:10.1038/s41598-018-33513-9
- 273 Härdle, W. and Simar, L. (2007). Canonical Correlation Analysis. In *Applied Multivariate Statistical*
274 *Analysis* (Berlin, Heidelberg: Springer Berlin Heidelberg). 321–330. doi:10.1007/978-3-540-72244-1\
275 _14
- 276 [Dataset] Häusser, M., Spruston, N., and Stuart, G. J. (2000). Diversity and dynamics of dendritic signaling.
277 doi:10.1126/science.290.5492.739
- 278 Hay, E., Hill, S., Schürmann, F., Markram, H., and Segev, I. (2011). Models of Neocortical Layer
279 5b Pyramidal Cells Capturing a Wide Range of Dendritic and Perisomatic Active Properties. *PLoS*
280 *Computational Biology* 7, e1002107. doi:10.1371/journal.pcbi.1002107
- 281 Intrator, N. and Cooper, L. N. (1992). Objective function formulation of the BCM theory of visual
282 cortical plasticity: Statistical connections, stability conditions. *Neural Networks* 5, 3–17. doi:10.1016/
283 S0893-6080(05)80003-6
- 284 [Dataset] Larkum, M. (2013). A cellular mechanism for cortical associations: An organizing principle for
285 the cerebral cortex. doi:10.1016/j.tins.2012.11.006

- 286 Larkum, M. E., Nevian, T., Sandier, M., Polsky, A., and Schiller, J. (2009). Synaptic integration
287 in tuft dendrites of layer 5 pyramidal neurons: A new unifying principle. *Science* 325, 756–760.
288 doi:10.1126/science.1171958
- 289 Law, C. C. and Cooper, L. N. (1994). Formation of receptive fields in realistic visual environments
290 according to the Bienenstock, Cooper, and Munro (BCM) theory. *Proceedings of the National Academy*
291 *of Sciences of the United States of America* 91, 7797–7801. doi:10.1073/pnas.91.16.7797
- 292 Lee, D. H., Zhang, S., Fischer, A., and Bengio, Y. (2015). Difference target propagation. In *Lecture Notes*
293 *in Computer Science (including subseries Lecture Notes in Artificial Intelligence and Lecture Notes in*
294 *Bioinformatics)* (Springer Verlag), vol. 9284, 498–515. doi:10.1007/978-3-319-23528-8_31
- 295 Letzkus, J. J., Kampa, B. M., and Stuart, G. J. (2006). Learning Rules for Spike Timing-Dependent
296 Plasticity Depend on Dendritic Synapse Location. *Journal of Neuroscience* 26, 10420–10429. doi:10.
297 1523/JNEUROSCI.2650-06.2006
- 298 Lillicrap, T. P., Cownden, D., Tweed, D. B., and Akerman, C. J. (2016). Random synaptic feedback
299 weights support error backpropagation for deep learning. *Nature Communications* 7, 1–10. doi:10.1038/
300 ncomms13276
- 301 Markram, H., Lübke, J., Frotscher, M., and Sakmann, B. (1997). Regulation of synaptic efficacy by
302 coincidence of postsynaptic APs and EPSPs. *Science* 275, 213–215. doi:10.1126/science.275.5297.213
- 303 Park, J., Papoutsi, A., Ash, R. T., Marin, M. A., Poirazi, P., and Smirnakis, S. M. (2019). Contribution
304 of apical and basal dendrites to orientation encoding in mouse v1 l2/3 pyramidal neurons. *Nature*
305 *communications* 10, 1–11
- 306 Poirazi, P. (2009). Information processing in single cells and small networks: Insights from compartmental
307 models. In *AIP Conference Proceedings* (American Institute of Physics), vol. 1108, 158–167. doi:10.
308 1063/1.3117124
- 309 [Dataset] Ramaswamy, S. and Markram, H. (2015). Anatomy and physiology of the thick-tufted layer 5
310 pyramidal neuron. doi:10.3389/fncel.2015.00233
- 311 Schiess, M., Urbanczik, R., and Senn, W. (2016). Somato-dendritic Synaptic Plasticity and Error-
312 backpropagation in Active Dendrites. *PLoS Computational Biology* 12, 1004638. doi:10.1371/journal.
313 pcbi.1004638
- 314 Schubert, F. and Gros, C. (2021). Local homeostatic regulation of the spectral radius of echo-state networks.
315 *Frontiers in computational neuroscience* 15, 12
- 316 Shai, A. S., Anastassiou, C. A., Larkum, M. E., and Koch, C. (2015a). Physiology of Layer 5
317 Pyramidal Neurons in Mouse Primary Visual Cortex: Coincidence Detection through Bursting. *PLOS*
318 *Computational Biology* 11
- 319 Shai, A. S., Anastassiou, C. A., Larkum, M. E., and Koch, C. (2015b). Physiology of Layer 5
320 Pyramidal Neurons in Mouse Primary Visual Cortex: Coincidence Detection through Bursting. *PLOS*
321 *Computational Biology* 11
- 322 Sjöström, P. J. and Häusser, M. (2006). A Cooperative Switch Determines the Sign of Synaptic Plasticity
323 in Distal Dendrites of Neocortical Pyramidal Neurons. *Neuron* 51, 227–238. doi:10.1016/j.neuron.2006.
324 06.017
- 325 Spruston, N. (2008). Pyramidal neurons: dendritic structure and synaptic integration. *Nature Reviews*
326 *Neuroscience* 9, 206–221. doi:10.1038/nrn2286
- 327 Spruston, N., Schiller, Y., Stuart, G., and Sakmann, B. (1995). Activity-dependent action potential invasion
328 and calcium influx into hippocampal CA1 dendrites. *Science* 268, 297–300. doi:10.1126/science.
329 7716524

- 330 Stuart, G. J. and Häusser, M. (2001). Dendritic coincidence detection of EPSPs and action potentials.
331 *Nature Neuroscience* 4, 63–71. doi:10.1038/82910
- 332 Urbanczik, R. and Senn, W. (2014). Learning by the Dendritic Prediction of Somatic Spiking. *Neuron* 81,
333 521–528. doi:10.1016/j.neuron.2013.11.030
- 334 Weissenberger, F., Gauy, M. M., Lengler, J., Meier, F., and Steger, A. (2018). Voltage dependence of
335 synaptic plasticity is essential for rate based learning with short stimuli. *Scientific Reports* 8, 4609.
336 doi:10.1038/s41598-018-22781-0